Journal of Sound and Vibration (2001) **244**(3), 407–430
doi:10.1006/jsvi.2000.3474, available online at http://www.idealibrary.com on IDEAL®

CALCULATING THE DYNAMIC STRAIN TENSOR FIELD USING MODAL ANALYSIS AND NUMERICAL DIFFERENTIATION

N. SEHLSTEDT

The Aeronautical Research Institute of Sweden, P.O. Box 11021, *SE*-161 11 *Bromma, Sweden.*
E-mail: stn@ffa.se

(*Received* 28 *January* 2000, *and in final form* 23 *August* 2000)

Based on vibration response measured at a limited number of points and continuous Hilbert space basis functions combined with spatial differentiation, a new method for strain tensor field assessment, in the frequency domain, is proposed. Essentially, results from hybrid modal analysis (HMA), are transformed from the displacement space to the strain space by use of finite difference schemes. This approach will produce a continuous strain (second order) tensor, except on a number of surfaces where material discontinuities are present.

Hybrid strain analysis (HSA), interpreted as dynamic strain analysis based on HMA, may be done in several ways. The method proposed here is the first realization of HSA and it has been verified by an experimental test case. The predicted results correspond well with measured strain responses.

The method is applicable to a vibrating structure, regardless of the material properties of the body. Hence, any possible damping, e.g., material damping, damping in joints between structural parts, etc., need not be known *a priori*. Moreover, the zero frequency elastic properties and mass distribution of the structure need not be the true ones; any (meaningful) arbitrary values of the elastic properties and mass distribution can be assumed in order to obtain the Hilbert space basis functions. Material inhomogeneities present, i.e., in a piecewise continuous structure, will cause the method (when applied with unknown material properties) to be somewhat inaccurate in the vicinity around the discontinuity. The derived model is valid for a specific excitation, not necessarily known.

1. INTRODUCTION

One important research field within the discipline of structural dynamics and vibroacoustics is characterization of the spatial distribution of dynamic displacement/strain/stress fields. In engineering applications, such as cars, ships and aircrafts, high strain/stress levels can, when occurring under a (long) period of time, cause failure from fatigue.

Detailed spatial characterization requires, when based on experimental data alone, a large number of measurements at a large number of points. To reduce costs it is thus desirable to use a minimal amount of experimental data, i.e., as few measurements and measurement points as possible. The contradictory demands for high spatial resolution and less extensive measurements may to some extent be solved using the hybrid modal analysis (HMA) technique [1]. The HMA technique is based on a restricted set of measured vibrations (acceleration, velocity or displacement), a knowledge of the geometry of the structure studied and on a set of numerically approximated three-dimensional, spatial basis

0022-460X/01/280407 + 24 $35.00/0

functions which are characteristic and well suited for the geometry of the part of the vibrating structure studied. In this context characteristic and well-suited means that the basis functions should satisfy any homogeneous essential boundary conditions for the displacement. Having such basis functions and applying HMA to a vibrating structure, the spatial distribution of the dynamic displacement field may be obtained. Here and in the following, spatial basis functions and elastic (normal) displacement (eigen) modes are used synonymously.

In the HMA technique, numerical approximations of elastic (continuous) displacement modes are used to supplement measured vibrations with information that enhances the spatial resolution of the measured data. Numerical approximations of the modes can be obtained by, for example, the finite element method (FEM). Due to the detailed spatial information which may be contained in these modes, the amount of measured data needed may be drastically reduced, for a given or desired spatial resolution, as long as the spatial distribution and number of measurement points is such that they can resolve the shortest wavelength of the spatial basis functions used. Typical applications of the technique is extrapolation of measured data to actual responses not measured; see Dovstam [1], and as an intermediate step in damping estimations [2]. It should be stressed that the technique is applicable, at a specific excitation (not necessarily known), independently of the material properties and that only the geometry of the vibrating body together with the measured data and the co-ordinates of the measurement points need to be known. Accurate geometrical description implies easily accessible, accurate basis functions defined as approximations to well-defined normal modes of vibration.

A natural extension, as proposed by Dovstam [3], of the HMA is hybrid strain analysis (HSA), where the displacement field, obtained by HMA, is spatially differentiated using, for example, numerical differentiation. Strain measurements with conventional strain gauges are not always possible. Moreover, they are also expensive, since the gauges are not reusable and cannot be moved from point to point when they have been attached to the structure. Thus, the need for alternative approaches is crucial for obtaining the strain tensor field, with a limited number of measurement points.

The objective of the work behind this paper is development and validation (experimentally) of hybrid strain analysis based on numerical differentiation. It is of great importance to obtain a method that yields the detailed dynamic strain tensor field regardless of the material properties, such as damping present, and also the possibility to predict the strain tensor where measurements are impossible or too involved.

Using the method proposed in this paper will produce the strain tensor at arbitrary points in the structure, regardless of the number of measured vibration responses; as long as the spatial distribution and number of measurement points fulfill the requirement to resolve the shortest wavelength of the vibrations.

In Bernasconi and Ewins [4], an approach, in the time domain, for determining the strain/stress field is outlined. They derive the strain tensor field in a body, but the derivation is restricted to the case with proportional damping and known material properties. Koss and Karczub [5] propose a method that concerns bending strain assessment using only two accelerometers for an Euler–Bernouilli beam; it is a one-dimensional method and therefore limited in its use. Camden and Simmons [6] establish the linear (one-dimensional) displacement–strain relationship for a specific structure and application.

In Karczub and Norton [7] the bending strain in an Euler–Bernouilli beam is again under study; this time the approach is based on finite difference schemes for the second order derivative of the transverse displacement, i.e., the curvature of the beam. The schemes are equidistant, and the measurement points are symmetrically distributed around the point of interest; hence, as they concluded, strain cannot be predicted at boundaries. Cuschieri [8]

proposes an experimental technique to measure the structural intensity through an aircraft fuselage; the technique involves estimation of the curvature by means of finite difference schemes and discrete measurement points. Lee and Kim [9] studied the normal and shear strains in a plate with a viscoelastic core layer. The strains are calculated using finite difference schemes on analytically obtained flexural vibrations of the plate with simple support. Also they assume that the viscoelastic layer does not have frequency-dependent material properties.

Throughout the text the three-dimensional displacement field in the time domain is denoted by $\mathbf{u}(\mathbf{x}, t)$, and its frequency domain, Laplace transformed, counterpart is denoted with a *tilde* above the function, i.e., $\tilde{\mathbf{u}}(\mathbf{x}, s)$. Here, and in the following, $s = \alpha + \mathrm{i}\omega$ is a complex frequency variable where i, $\mathrm{i}^2 = -1$, denotes the imaginary unit and ω is the circular frequency (rad/s) of vibration.

2. GOVERNING EQUATIONS

Consider a three-dimensional solid occupying a volume $\Omega \subset \mathbb{R}^3$; strictly mathematically speaking Ω is a compact set, i.e., a closed and bounded set. The vibrations of the vibrating body may be described by a three-dimensional displacement field $\mathbf{u} = \mathbf{u}(\mathbf{x}, t)$ where $\mathbf{x}$ is a point in the body, and t is the time variable. If vanishing body forces are assumed, the time domain, linearized equations of motion are given by

$$-\mathbf{D}^{\mathrm{T}}[\boldsymbol{\sigma}] + \rho\ddot{\mathbf{u}} = \mathbf{0}, \tag{1}$$

where $\rho = \rho(\mathbf{x})$ is the mass distribution, $\boldsymbol{\sigma} = \boldsymbol{\sigma}(\mathbf{x}, t)$ is the Voight-matrix representation of the stress tensor, and $\mathbf{D}$ is the linear (strain) partial differential operator defined in Appendix A, and discussed in Appendix B.

The Laplace transformed frequency domain (s-domain) counterpart of equation (1) can now be expressed as

$$-\mathbf{D}^{\mathrm{T}}[\tilde{\boldsymbol{\sigma}}] + s^2\rho\tilde{\mathbf{u}} = \mathbf{0}, \tag{2}$$

where $\tilde{\boldsymbol{\sigma}} = \tilde{\boldsymbol{\sigma}}(\mathbf{x}, s)$ and $\tilde{\mathbf{u}} = \tilde{\mathbf{u}}(\mathbf{x}, s)$ are the frequency domain stress and displacement fields respectively.

For a linear material at isothermal, but otherwise general conditions, the stress–strain relationship can be described by

$$\tilde{\boldsymbol{\sigma}} = \hat{\mathbf{H}}\tilde{\boldsymbol{\varepsilon}}, \tag{3}$$

where $\hat{\mathbf{H}} = \hat{\mathbf{H}}(\mathbf{x}, s)$ is a complex, position and frequency dependent constitutive 6×6 material matrix; $\tilde{\boldsymbol{\varepsilon}} = \tilde{\boldsymbol{\varepsilon}}(\mathbf{x}, s)$ is the frequency domain strain field. Assume that $\hat{\mathbf{H}}$ can be decomposed as (see e.g., references [1, 10])

$$\hat{\mathbf{H}} = \mathbf{H} + \mathbf{H}_{\Delta} = \bar{\mathbf{H}} + \delta\mathbf{H} + \mathbf{H}_{\Delta}, \tag{4}$$

where $\mathbf{H} = \bar{\mathbf{H}} + \delta\mathbf{H}$ and $\mathbf{H}_{\Delta}$ denote the true zero frequency, relaxed elastic properties, and the frequency-dependent anelastic properties respectively. $\bar{\mathbf{H}}$ and $\delta\mathbf{H}$ are the assumed, arbitrary zero frequency elastic properties and the deviation from the true elastic zero frequency properties respectively.

3. DISPLACEMENT PREDICTIONS

Modelling and prediction of vibrations and acoustical behaviour in practice have to be done using finite dimensional (or discrete) models. Since the discrete model always is an approximation of the continuous system, it is of great importance to choose a model that approximates the system well enough. Today, discrete models are derived in engineering applications using experimental modal analysis (see e.g., reference [11]). In reference [1] a new technique that combines continuous elastic (normal) modes of vibration and experimentally measured vibration responses is proposed. The technique is named hybrid modal analysis (HMA) and it will produce the three-dimensional displacement field at arbitrary points in the structure. In this section a short summary of the basic results and ideas behind HMA will be given.

3.1. MODE SERIES EXPANSION AND SPATIAL BASIS FUNCTIONS

In the frequency domain the Laplace transformed displacement field, $\tilde{\mathbf{u}}$, may be represented by generalized Fourier series

$$\tilde{\mathbf{u}}(\mathbf{x}, s) = \tilde{\mathbf{u}}_M(\mathbf{x}, s) + \tilde{\mathbf{u}}_{res}(\mathbf{x}, s), \tag{5}$$

$$\tilde{\mathbf{u}}_M(\mathbf{x}, s) = \sum_{m=1}^{M} c_m(\tilde{\mathbf{u}})\mathbf{w}^{(m)}(\mathbf{x}), \tag{6}$$

where $\tilde{\mathbf{u}}_{res}(\mathbf{x}, s)$ is the pointwise error, or residual. Hence, the displacement field can be approximated by $\tilde{\mathbf{u}}(\mathbf{x}, s) \approx \tilde{\mathbf{u}}_M(\mathbf{x}, s)$. The three-dimensional real vector field $\mathbf{w}^{(m)} \in \mathbb{R}^3$ is the mode shape number m with corresponding circular eigenfrequency ω_m satisfying a suitable elastic eigenvalue problem (see Appendix A). The sequence $\{\mathbf{w}^{(m)}\}_{m=1}^{\infty}$ is known to be complete in the Hilbert space $\mathbf{L}_2^3(\Omega)$ (see Appendix A).

The s-dependent, i.e., frequency dependent, coefficients $c_m(\tilde{\mathbf{u}})$ in equation (6), are linear functionals of the Laplace transformed displacement field $\tilde{\mathbf{u}}$ defined as

$$c_m(\tilde{\mathbf{u}}) = (\tilde{\mathbf{u}}, \rho\mathbf{w}^{(m)})/a_m, \qquad a_m = (\mathbf{w}^{(m)}, \rho\mathbf{w}^{(m)}) > 0, \tag{7, 8}$$

$\forall m \in \mathbb{N}$. ρ is the mass distribution of the structure and $(\mathbf{u}, \mathbf{v})$ denotes the inner product, in the function space $\mathbf{L}_2^3(\Omega)$ (see Appendix A). Equation (7) may be used when the whole field $\tilde{\mathbf{u}}$ and ρ are known [12].

It is important to note that since it is only required that the modes $\mathbf{w}^{(m)}$ constitute a complete set of basis functions, the elastic constants (G and λ for an isotropic material) and the mass distribution, ρ, need not be the actual ones for the continuum occupying the volume Ω. Hence, any meaningful value of the elastic constants and the mass distribution is sufficient in order to obtain the modes, $\mathbf{w}^{(m)}$. As a consequence, the material properties of the structure in question need not be known, to get good results, when using hybrid modal analysis as outlined in this section.

3.2. HYBRID MODAL ANALYSIS

Consider a finite dimensional response model [1], with N responses. The displacement response, $\tilde{U}_i$, in a direction $\hat{\mathbf{n}}_i$, at a certain point $P(i)$, with co-ordinate vector $\mathbf{x}_{P(i)}$ in the

discrete model may be expressed as

$$\tilde{U}_i = \sum_{k=1}^{K} R_{ik} \tilde{F}_k, \tag{9}$$

where K is the total number of excitation points and R_{ik} are receptances defined by the quotient spectra

$$R_{ik} = \frac{\tilde{u}_{n(i)}(\mathbf{x}_{P(i)}, s)}{\tilde{F}_k(s)}, \tag{10}$$

where $\tilde{u}_{n(i)}(\mathbf{x}_{P(i)}, s) = \hat{\mathbf{n}}_i \cdot \tilde{\mathbf{u}}(\mathbf{x}_{P(i)}, s)$.

Now, let the vector $\tilde{\mathbf{U}} = \tilde{\mathbf{U}}(s)$ correspond to the finite dimensional response model with component spectrum $\tilde{U}_i(s)$ defined by a number N of measured degrees of freedom. Also let M be the number of normal modes in a modal expansion of $\tilde{\mathbf{u}}$, as in equation (6). Then, a real and constant, modal $N \times M$ response matrix $\mathbf{A}$ is defined such that

$$\tilde{\mathbf{U}} = \mathbf{A}\tilde{\mathbf{C}} + \tilde{\mathbf{U}}_{res}, \qquad A_{im} = \hat{\mathbf{n}}_i \cdot \mathbf{w}^{(m)}(\mathbf{x}_{P(i)}), \tag{11, 12}$$

$$\tilde{\mathbf{C}} = [c_1(\tilde{\mathbf{u}}), c_2(\tilde{\mathbf{u}}), \ldots, c_M(\tilde{\mathbf{u}})]^{\mathrm{T}}, \qquad \tilde{\mathbf{U}}_{res} = \mathbf{A}^{res}\tilde{\mathbf{C}}^{res}, \tag{13, 14}$$

$\mathbf{A}^{res}$ and $\tilde{\mathbf{C}}^{res}$ are defined in analogy with equations (12) and (13).

From equation (11) follows that the coefficient spectra can be estimated by

$$\tilde{\mathbf{C}}_{est} = \mathbf{A}^{+}(\tilde{\mathbf{U}} - \tilde{\mathbf{U}}_{res}), \tag{15}$$

where $\mathbf{A}^{+}$ is the pseudoinverse of $\mathbf{A}$. Estimates for the residual, $\tilde{\mathbf{U}}_{res}$, in equation (15) are discussed in section 4.

Now a vibration response, which is not measured, at a point $\mathbf{y} \in \Omega$ can be predicted using the equation

$$\tilde{\mathbf{u}}_{pred}(\mathbf{y}, s) = \mathbf{W}(\mathbf{y})\tilde{\mathbf{C}}_{est} + \tilde{\mathbf{u}}_{res}(\mathbf{y}, s), \tag{16}$$

where $\mathbf{W}(\mathbf{y})$ is the $3 \times M$ modal matrix defined as

$$\mathbf{W}(\mathbf{y}) = [\mathbf{w}^{(1)}(\mathbf{y}), \mathbf{w}^{(2)}(\mathbf{y}), \ldots, \mathbf{w}^{(M)}(\mathbf{y})] = \begin{bmatrix} w_1^{(1)} & w_1^{(2)} & \cdots & w_1^{(M)} \\ w_2^{(1)} & w_2^{(2)} & \cdots & w_2^{(M)} \\ w_3^{(1)} & w_3^{(2)} & \cdots & w_3^{(M)} \end{bmatrix}. \tag{17}$$

Equations (11)–(16) constitute the basic concepts of hybrid modal analysis (HMA). The responses $\tilde{U}_i$ in $\tilde{\mathbf{U}}$ are thus identified by a number, N, of measured responses, and the corresponding modal response matrix $\mathbf{A}$, as in equation (12), is constructed from the basis functions $\mathbf{w}^{(m)}$.

3.3. SECTION SUMMARY

The spatial basis functions, $\mathbf{w}^{(m)}$, are obtained by solving the elastic eigenvalue problem; displacement (or acceleration/velocity transformed to displacement) vibration responses,

$\tilde{U}_i$, are measured on the structure at discrete points, $P(i)$; thereafter a least-squares fit of the Fourier coefficients, $c_m(\tilde{\mathbf{u}})$, is obtained by using equation (15). Now the displacement vector, $\tilde{\mathbf{u}}$, can be predicted anywhere in the structure using equation (16); i.e., since $\mathbf{W}(\mathbf{y})$ is available at some (high) number of points in the structure (e.g., decided by the FE-net) and combined with interpolation, displacement at arbitrary points in the structure can be predicted.

4. RESIDUAL AND RESPONSE MODEL

In the general case, different coefficients $c_m(\tilde{\mathbf{u}})$ of equation (6) are not independent; i.e., the modes are coupled. For a linear structure, coupling may occur due to damping and deviations between $\bar{\mathbf{H}}$ and the true elastic (zero frequency) modulus matrix, $\mathbf{H} = \bar{\mathbf{H}} + \delta\mathbf{H}$; even if the series is not truncated, coupling may occur. Also, the material properties are unknown in a typical application of HSA and HMA, and the modes should therefore, in general, be assumed to be coupled.

Situations in real-world applications where the "true" modes are completely uncoupled are quite rare, though there are many cases where they are almost uncoupled. One example is when the anelastic properties are proportional to the elastic properties, e.g., as in the case of classical Rayleigh damping.

Although it is not known what the true residual, $\tilde{\mathbf{U}}_{res}$, looks like, it may in some cases be approximated as uncoupled. Another approach would be to include a large number of modes in the coefficient estimation, i.e., large M in equations (11)–(14), and neglect the residual completely. The number of measurements, N, must then also be increased for the system of equations to be sufficiently overdetermined. Here overdetermined means that the number of measurements, N, should be large compared to the number of modes, M, so that the estimated Fourier coefficients are smooth enough in the frequency interval of interest.

In an application where the excitation is not known, there is no way of estimating the residual. Hence, it must be neglected and a large number of modes should be included in the coefficient estimation.

4.1. MODEL BASED ON UNKNOWN MATERIAL PROPERTIES

Let $\bar{\rho}$ be some arbitrary mass distribution, and $\bar{\mathbf{H}}$ be the assumed zero frequency elastic material properties, as defined in section 2. Then solving the elastic eigenvalue problem with the above material properties, gives the modal circular eigenfrequencies, $\bar{\omega}_m$, and the normal modes, $\bar{\mathbf{w}}^{(m)}$. The *bar* above each variable denotes that it is derived with some assumed material properties.

Then taking the inner product between the equations of motion (2) and $\bar{\mathbf{w}}^{(m)}$, and using the stress–strain relationship (3) and equations (4), (7), (A.17) and (A.18) it follows after partial integration that

$$c_m(\tilde{\mathbf{u}}) = \frac{\tilde{F}_{\partial}^{(m)}(s) - \kappa_{\Delta}^{(m)}(s) - \kappa_{\delta}^{(m)}(s)}{\bar{a}_m(\bar{\omega}_m^2 + s^2)}, \tag{18}$$

where the modal force $\tilde{F}_{\partial}^{(m)}(s)$ is given as

$$\tilde{F}_{\partial}^{(m)}(s) = (\tilde{t}_n, \bar{\mathbf{w}}^{(m)})_{\partial} \tag{19}$$

with $(\cdot,\cdot)_\partial$ defined in Appendix A, and $\tilde{\mathbf{t}}_n$ is the Cartesian traction vector also defined in Appendix A. For point force excitation at point $\mathbf{x}_e$ acting along the x_k-axis, $\tilde{F}_\partial^{(m)}(s) = \tilde{F}_k(s)\cdot\bar{w}_k^{(m)}(\mathbf{x}_e)$.

The functionals $\kappa_\Delta^{(m)}(s)$ and $\kappa_\delta^{(m)}(s)$ in equation (18) are defined as

$$\kappa_\Delta^{(m)}(s) = \langle \mathbf{H}_\Delta \tilde{\boldsymbol{\varepsilon}}, \bar{\boldsymbol{\varepsilon}}^{(m)} \rangle, \tag{20}$$

$$\kappa_\delta^{(m)}(s) = \langle \delta\mathbf{H} \tilde{\boldsymbol{\varepsilon}}, \bar{\boldsymbol{\varepsilon}}^{(m)} \rangle, \tag{21}$$

where $\langle \cdot,\cdot \rangle$ is the inner product for six-dimensional vector fields as defined in Appendix A, and $\tilde{\boldsymbol{\varepsilon}}$ is the current strain vector field due to the actual excitation, $\bar{\boldsymbol{\varepsilon}}^{(m)} = \mathbf{D}[\bar{\mathbf{w}}^{(m)}]$ is the elastic strain mode, and $\mathbf{H}_\Delta$ and $\delta\mathbf{H}$ are defined in section 2. It can be seen, from equations (20) and (21), that since both functionals $\kappa_\Delta^{(m)}(s)$ and $\kappa_\delta^{(m)}(s)$ depend on the whole current strain vector field $\tilde{\boldsymbol{\varepsilon}}$, the coefficients $c_m(\tilde{\mathbf{u}})$ are, in general, coupled.

Equation (18) is analogous to Dovstam [1, equation (52)]. The only difference is that the true mass distribution is not assumed to be known.

It is clear, from equations (20) and (21), that $\kappa_\Delta^{(m)}(s)$ and $\kappa_\delta^{(m)}(s)$ depend on respective the damping present and the deviation from the true elastic zero frequency modulus matrix. Long strain (the *true* current strain at frequency s) wavelengths combined with short wavelength natural *modes* cause $\kappa_\Delta^{(m)}(s)$ and $\kappa_\delta^{(m)}(s)$ to be small; hence they may be neglected in some cases for high order modes. A one-dimensional example of this is a strain field $\bar{\varepsilon} = \sin(\pi x)$ and elastic strain mode $\bar{\varepsilon}^{(m)} = \sin(m\pi x)$ in the domain $x \in [0, a]$. Then $\kappa_\delta^{(m)}(s)$ is small for high values of m and arbitrary values of a.

With rigid-body modes present it follows from equation (18) that the Fourier coefficients, $c_m(\tilde{\mathbf{u}})$, for the rigid-body modes are given explicitly as

$$c_m(\tilde{\mathbf{u}}) = -\frac{\tilde{F}_k(s)\cdot\bar{w}_k^{(m)}(\mathbf{x}_e)}{\bar{a}_m\omega^2}, \tag{22}$$

since $\bar{\omega}_m \equiv 0$, $s = \mathrm{i}\omega$ and $\bar{\boldsymbol{\varepsilon}}^{(m)} \equiv \mathbf{0}$ for those modes. Note that in an application with unknown excitation the Fourier coefficients for the rigid-body modes must be estimated using equation (15).

Now, since it is generally not possible to say anything about the damping part, $\kappa_\Delta^{(m)}$, nor the elastic deviation part, $\kappa_\delta^{(m)}$, one possible way to proceed is to neglect them and use as many modes, M, as possible. The response, due to a point force with unit spectrum $\tilde{F}_k(s) = 1$, is then expressed as

$$r_{ik} \approx \sum_{m=1}^{M} c_m(\tilde{\mathbf{u}})\bar{w}_i^{(m)}(\mathbf{x}) + \sum_{m=M+1}^{m_{max}} \frac{\bar{w}_i^{(m)}(\mathbf{x})\bar{w}_k^{(m)}(\mathbf{x}_e)}{\bar{a}_m(\bar{\omega}_m^2 + s^2)}, \tag{23}$$

where $r_{ik} = \bar{u}_i(\mathbf{x}, s)/\tilde{F}_k(s)$, and m_{max} is some positive integer (i.e., the maximum number of modes available). Another obvious possibility is to neglect the whole numerator, $\tilde{F}_\partial^{(m)}(s) - \kappa_\Delta^{(m)}(s) - \kappa_\delta^{(m)}(s)$, in equation (18) for all m larger than M, i.e., to use equation (6) directly with a large enough M.

Now, the response model, with six rigid-body modes, to be used in the following can be given as:

$$R_{ik}(\omega) \approx -\sum_{m=1}^{6} \frac{\bar{w}_i^{(m)}(\mathbf{x}_{P(i)})\bar{w}_k^{(m)}(\mathbf{x}_e)}{\bar{a}_m\omega^2} + \sum_{m=7}^{M} \bar{w}_i^{(m)}(\mathbf{x}_{P(i)})C_m(\omega) + Res_{ik}, \tag{24}$$

where $R_{ik}(\omega)$ is defined according to equation (10), $C_m(\omega) = (c_m(\tilde{\mathbf{u}}))_{s=i\omega}$ and Res_{ik}, when included, is the residual defined as

$$Res_{ik} = \sum_{m=M+1}^{m_{max}} \frac{\bar{w}_i^{(m)}(\mathbf{x}_{P(i)})\bar{w}_k^{(m)}(\mathbf{x}_e)}{\bar{a}_m(\bar{\omega}_m^2 - \omega^2)}. \tag{25}$$

4.2. SECTION SUMMARY

In this section the residual and response model were examined in detail for the case with point force excitation, though the expression in equation (18) is generally valid for any type of excitation. In most applications the residual, as in equation (25), may or has to be neglected completely. An indication of this will be noticed when comparing the predicted vibration (displacement) response with and without the residual, using equation (24), with independently measured vibration (displacement, or velocity, acceleration transformed into displacement) spectrum.

5. DYNAMIC STRAIN ASSESSMENT

An accurate representation of the dynamic displacement field can now be obtained using the results from the previous sections. In this section, a method that combines the results from the above sections with numerical spatial differentiation is outlined. This is the first realization of a class of methods [3], called hybrid strain analysis (HSA).

The idea behind the method is to obtain the strain tensor in a vibrating structure without the use of conventional strain gauges. Vibration (displacement, velocity or acceleration) frequency response function (FRF) measurements are carried out on the structure. It must be emphasized that measurements must be carried out so that the spatial distribution and number of measurement points is chosen such that it is possible to resolve the shortest wavelength of the vibration field, $\tilde{\mathbf{u}}$, to be characterized, which influences the choice of the displacement modes, $\mathbf{w}^{(m)}$ $m \in [1, \ldots, M]$, used in the modal expansion (6). Thereafter, the complete displacement field of the body in question, or a part of it, can be obtained by means of HMA. With the use of finite difference schemes the strain tensor can be calculated for the whole body, or just certain parts/points of interest.

By means of given displacements and finite difference schemes the strain tensor can be approximated to any degree of accuracy due to Weierstrass approximation theorem [13]. Predicted displacement responses, obtained by HMA, at a finite number of points adjacent to the point in question are utilized in the finite difference procedure. The computational cost can in this way be kept to a minimum without loss of accuracy.

The requirements for HMA are: an accurate geometrical description of the structure; measured vibrations including measurement direction and the co-ordinates for the measurement points. For HSA this is also true, but if material discontinuities are present (as for built-up, piecewise continuous structures), the number of modes, used in the modal expansion (6), must be increased in order to describe the discontinuity of the strain tensor, and thus also the number of measured responses must be increased. However, if the "true" zero frequency elastic material properties and mass distribution are known, HSA may produce accurate results, even in the vicinity of the material discontinuity, without increasing the number of modes.

5.1. HYBRID STRAIN ANALYSIS

The Eulerian finite strain tensor in Cartesian co-ordinates is defined as (see reference [14])

$$\varepsilon_{ij} = \frac{1}{2}\left(\frac{\partial u_i}{\partial x_j} + \frac{\partial u_j}{\partial x_i} - \frac{\partial u_k}{\partial x_i}\frac{\partial u_k}{\partial x_j}\right), \tag{26}$$

where the summation convention is used; i.e., sum on index k. The strain tensor field, $\boldsymbol{\varepsilon} = \boldsymbol{\varepsilon}(\mathbf{x}, t)$, describes the strain of the body in the time domain; the frequency domain counterpart is denoted as $\tilde{\boldsymbol{\varepsilon}} = \tilde{\boldsymbol{\varepsilon}}(\mathbf{x}, s)$.

In most applications the strain tensor, as in equation (26), is approximated as linear; i.e., the last term of equation (26) is neglected. Calculating the strain tensor field, $\tilde{\boldsymbol{\varepsilon}}$, from the displacement field, $\tilde{\mathbf{u}}$, in a three-dimensional body thus involves calculations of nine different first order derivatives.

Since the complete displacement field in the frequency domain, $\tilde{\mathbf{u}}$, is available through the use of HMA, an approximation of the strain tensor field in the frequency domain can be obtained through numerical spatial differentiation of the estimated field $\tilde{\mathbf{u}}$, by use of, for example, finite difference schemes. When the elastic modes, $\mathbf{w}^{(m)}(\mathbf{x})$, are obtained through finite element calculations, the spatial node distribution in the finite element mesh is in general non-equidistant; in reference [15] finite difference schemes for three and five non-equidistant distributed node points were derived. An example of this, for the calculation of the linear strain tensor component, $\tilde{\varepsilon}_{11}$, with a three-point (that is, order two) forward difference scheme is

$$\tilde{\varepsilon}_{11}(\mathbf{x}_0, s) = -\tilde{u}_1(\mathbf{x}_0, s)\frac{2h_1 + h_2}{h_1(h_1 + h_2)} + \tilde{u}_1(\mathbf{x}_1, s)\frac{h_1 + h_2}{h_1 h_2} - \tilde{u}_1(\mathbf{x}_2, s)\frac{h_1}{h_2(h_1 + h_2)}, \tag{27}$$

where h_1 and h_2 are the distances in the first (i.e., x_1) direction between $\mathbf{x}_0$ and $\mathbf{x}_1$, respectively, $\mathbf{x}_1$ and $\mathbf{x}_2$. By use of schemes for non-uniformly distributed nodes (i.e., forward and backward), the strain tensor on the boundary of the structure and on the interface between material discontinuities can be calculated.

Assume that a finite difference scheme of order n, i.e., $n + 1$ points, is to be used; then the hybrid strain analysis can be summarized as follows.

(1) Solution of an eigenvalue problem (as in equations (A.17) and (A.18)) for the body studied, with detailed geometrical description (i.e., a high number of finite elements) if HSA is based on the finite element method. The number of modes, M, in the mode series expansion should be chosen so that the residual approximation is as correct as possible (i.e., $m_{max} \gg M$), or such that the residual may be neglected (a matter of wavelength for number M used).
(2) Vibration FRF measurements at N number of points on the structure. N should be large enough compared with the number of modes M so that the system of equations, as in equation (11), is overdetermined enough, and so that the shortest wavelength of the vibration field, $\tilde{\mathbf{u}}$, and the basis fields, $\mathbf{w}^{(m)}$, can be resolved (see section 6).
(3) Residual approximation, if the excitation is known, using equation (25). If the number of modes, M, is high enough the residual can be neglected. Note that the residual approximation according to equation (25) can actually worsen the results. An indication of this will be noticed when validating the coefficient spectra, as in item (5).

(4) Fourier coefficient spectra estimation, by use of equation (15), and if the excitation is known by use of equation (22) for the rigid-body modes.
(5) Validation of coefficient spectra using equations (5) and (6), and independently measured spectra.
(6) Displacement response prediction at $3n + 1$ points (i.e., the point of interest and n adjacent points in each (Cartesian) co-ordinate direction) by use of equation (16) with residual part defined by equation (25), if not neglected.
(7) Strain tensor calculation using finite difference schemes of order n and equation (26).

Items (3) and (4) should, if possible, be done with and without residual, and comparison with independently measured spectra should be made for both according to item (5).

If the structure in question has a very complex geometry and the strain tensor is only sought on some local part of the structure, HSA can be performed on this local part; that is, the measurements need only be distributed over the local structure. This will be outlined in a forthcoming paper by the author.

5.2. SECTION SUMMARY

It cannot be emphasized enough that the strain tensor can easily be obtained at arbitrary points in the structure. This is an important consequence of the fact that the displacement field can be obtained anywhere in the structure, and thus the complete strain tensor field is easily obtained by use of finite difference schemes.

6. MEASUREMENTS AND NUMBER OF ELASTIC MODES

When measurements of a vibrating structure are to be performed, the question of the spatial distribution of measurement points always arises. In a situation with a specific, but arbitrary, displacement field $\tilde{\mathbf{u}}(\mathbf{x}, s)$ there is no possibility of knowing in advance the length of the waves of $\tilde{\mathbf{u}}$. On the other hand, when using HMA and HSA, as described in sections 3 and 5, respectively, there is implicit knowledge of the spatial wavelengths of the elastic eigenmodes $\mathbf{w}^{(m)}$. Therefore, some information of the needed spatial distribution of measurement points may be obtained from the eigenmode with shortest wavelength used, which is usually the eigenmode with highest mode number. The number of elastic eigenmodes used should always be validated using separately measured vibration (displacement) spectra. This will give some indication of the length of the waves of $\tilde{\mathbf{u}}(\mathbf{x}, s)$, i.e., if the predicted displacement field deviates (possibly due to aliasing; see reference [16]) from the measured, the number of elastic eigenmodes should be increased.

In three-dimensional space the minimum requirements, assuming that a high enough number of modes M has been chosen, is that the number of measurements, N, or (more exact) the maximum distance between the measurements, must be chosen so that the elastic eigenmode number M can be resolved in each co-ordinate direction. Explicitly, this should be satisfied with *more* than three measurements per wavelength for mode number M. For example, in a situation with two complete waves covering the length of a structure, there should be *at least* seven measurements distributed over the length.

When dealing with structures with unknown excitation and/or unknown zero frequency elastic material properties and mass distribution, especially with the case of built up piecewise continuous structures (a structure consisting of sub-structures with different material properties), it is very important to satisfy the minimum requirements of measurement point spacing (as discussed above) in *each* co-ordinate direction; otherwise the

predicted (strain/displacement) response may be inaccurate. In some cases, when the elastic material properties and mass distribution in a piecewise continuous structure is known, good results may be obtained even if the minimum requirements are not satisfied in one direction. This is due to the fact that the elastic eigenmodes represent the structural behaviour very well.

In applications with known zero frequency elastic properties and mass distribution, the number of modes, M, to be used in the modal expansion (6), is directly related to the frequency range of the analysis; that is, M is chosen so that $\omega < \omega_{max} < \omega_M$ with $\omega_{max} < \omega_{mea}$ where $f = \omega/2\pi$ and $\omega = \mathrm{Im}\{s\}$. f_{max} is the maximum frequency of interest, and f_{mea} is the maximum measured frequency.

7. CONVERGENCE AND SENSITIVITY TO PERTURBATIONS

The question of convergence or not is of great importance when dealing with series. Since the fields $\mathbf{w}^{(m)}$, $m = 1, 2, \ldots$, are assumed to constitute a complete set of normal modes, the Fourier series, as in equation (6), always converges [13] to $\tilde{\mathbf{u}}$ in the meaning

$$\lim_{M\to\infty} \|\tilde{\mathbf{u}}_M - \tilde{\mathbf{u}}\|_{\mathbf{L}_2^3(\Omega)} = \lim_{M\to\infty} \sqrt{(\tilde{\mathbf{u}}_M - \tilde{\mathbf{u}},\ \tilde{\mathbf{u}}_M - \tilde{\mathbf{u}})} = 0, \tag{28}$$

where $\|\cdot\|_{\mathbf{L}_2^3(\Omega)}$ is the $\mathbf{L}_2^3(\Omega)$ norm defined in Appendix A.

Due to equation (28), the mean value of the displacement field, $\tilde{\mathbf{u}}_{mean}$, over arbitrary small, but finite, volumes at each point $\mathbf{x} \in \Omega$, may be approximated by a sum, $\tilde{\mathbf{u}}_{M,mean}$, to any required accuracy [1]. For the definition of mean values see Appendix A. Hence, in the l_2-norm, as defined in Appendix A, at a point $\mathbf{p} \in \Omega$

$$\lim_{M\to\infty} \|\tilde{\mathbf{u}}_{M,mean} - \tilde{\mathbf{u}}_{mean}\|_{l_2} = 0. \tag{29}$$

Assuming that the strain–displacement relations are linear (i.e., the quadratic terms in equation (26) vanish) then the frequency domain strain–displacement relation at each point $\mathbf{p} \in \Omega$ can be described by

$$\tilde{\boldsymbol{\varepsilon}} = \mathbf{D}[\tilde{\mathbf{u}}], \tag{30}$$

where $\mathbf{D}$ is defined in Appendix A. For the mean value of the six-dimensional strain field, with l_2-norm defined in Appendix A, at a point $\mathbf{p} \in \Omega$, $\exists L$, $\forall \varepsilon > 0$ (L is finite) so that

$$\begin{aligned} \|\tilde{\boldsymbol{\varepsilon}}_{L,mean} - \tilde{\boldsymbol{\varepsilon}}_{mean}\|_{l_2} &= \|\mathbf{D}[\tilde{\mathbf{u}}_{L,mean}] - \mathbf{D}[\tilde{\mathbf{u}}_{mean}]\|_{l_2} \\ &\leqslant K \cdot \|\tilde{\mathbf{u}}_{L,mean} - \tilde{\mathbf{u}}_{mean}\|_{l_2} < \varepsilon, \end{aligned} \tag{31}$$

where the boundedness (Appendix B) of the strain operator (for piecewise continuously differentiable displacements) was used. K is a finite positive real number. (see Appendix B). Thus for a high number of modes L the predicted strain tensor is close to the true strain tensor. It is vital to keep in mind that mean convergence, as in equation (28), does *not*, in general, imply pointwise convergence; but it is known [13] that if $\tilde{\mathbf{u}}_M(\mathbf{x}, s)$ converges to $\tilde{\mathbf{u}}(\mathbf{x}, s)$ in $\mathbf{L}_2^3(\Omega)$ then there is a subsequence of $\tilde{\mathbf{u}}_M(\mathbf{x}, s)$ that converges to $\tilde{\mathbf{u}}(\mathbf{x}, s)$ for *almost* all $\mathbf{x} \in \Omega$.

It must be emphasized that the integer L must be finite for equation (31) to be valid. With L going to infinity, there will not, in general, be (pointwise) convergence. To see this consider a one-dimensional example with basis functions $u_L(x) = \sin(Lx)$ with derivative (or strain) $D[u_L] = L\cos(Lx)$ which will *not* be finite when L goes to infinity.

To be able to specify error bounds for the strain tensor calculated using HSA, studies must be made as to how perturbations in measured response affect the calculated strain tensor.

Let $\delta\tilde{\mathbf{U}} = \tilde{\mathbf{U}} - \tilde{\mathbf{U}}_{mea}$ be some error in the measured response of a vibrating structure. $\tilde{\mathbf{U}}$ is defined as in equation (11), and $\tilde{\mathbf{U}}_{mea}$ is the measured counterpart to $\tilde{\mathbf{U}}$. Fourier coefficient estimation, as in equation (15), for the true and measured response can be expressed as

$$\tilde{\mathbf{C}}_{est}^{true} = \mathbf{A}^+(\tilde{\mathbf{U}} - \tilde{\mathbf{U}}_{res}), \qquad \tilde{\mathbf{C}}_{est}^{mea} = \mathbf{A}^+(\tilde{\mathbf{U}}_{mea} - \tilde{\mathbf{U}}_{res}). \tag{32, 33}$$

Let $\mathbf{W}(\mathbf{x}) = [\mathbf{w}^{(1)}(\mathbf{x}), \mathbf{w}^{(2)}(\mathbf{x}), \ldots, \mathbf{w}^{(M)}(\mathbf{x})]$ be the $3 \times M$ modal matrix. Then the predicted displacement, $\tilde{\mathbf{u}}_{pred}$, can be expressed as

$$\tilde{\mathbf{u}}_{pred}(\mathbf{x}, s) = \mathbf{W}(\mathbf{x})\tilde{\mathbf{C}}_{est} + \tilde{\mathbf{u}}_{res}(\mathbf{x}, s) \tag{34}$$

for a point in the body, Ω with co-ordinate vector $\mathbf{x}$. Now the strain tensor can be calculated using equation (30). For the true and measured response the Voight-matrix representation of the strain tensors are, respectively,

$$\tilde{\boldsymbol{\varepsilon}}(\mathbf{x}, s) = \mathbf{D}[\mathbf{W}(\mathbf{x})]\tilde{\mathbf{C}}_{est}^{true} + \mathbf{D}[\tilde{\mathbf{u}}_{res}(\mathbf{x}, s)], \tag{35}$$

$$\tilde{\boldsymbol{\varepsilon}}_{mea}(\mathbf{x}, s) = \mathbf{D}[\mathbf{W}(\mathbf{x})]\tilde{\mathbf{C}}_{est}^{mea} + \mathbf{D}[\tilde{\mathbf{u}}_{res}(\mathbf{x}, s)]. \tag{36}$$

Subtract equation (36) from equation (35) and define $\delta\tilde{\boldsymbol{\varepsilon}} = \tilde{\boldsymbol{\varepsilon}} - \tilde{\boldsymbol{\varepsilon}}_{mea}$ as the pointwise error in the calculated strain tensor caused by error in the response measurements. This yields

$$\delta\tilde{\boldsymbol{\varepsilon}}(\mathbf{x}, s) = \mathbf{D}[\mathbf{W}(\mathbf{x})](\tilde{\mathbf{C}}_{est}^{true} - \tilde{\mathbf{C}}_{est}^{mea}) = D[\mathbf{W}(\mathbf{x})]\mathbf{A}^+\delta\tilde{\mathbf{U}}, \tag{37}$$

where in the last equality equations (32) and (33) were used. Using Cauchy–Schwarz' inequality and the l_2-norm on equation (37) gives the estimate

$$\|\delta\tilde{\boldsymbol{\varepsilon}}\|_{l_2} \leqslant \|\mathbf{D}[\mathbf{W}(\mathbf{x})]\|_{l_2} \cdot \|\mathbf{A}^+\|_{l_2} \cdot \|\delta\tilde{\mathbf{U}}\|_{l_3}. \tag{38}$$

Note that $\delta\tilde{\boldsymbol{\varepsilon}}$ is a six-dimensional vector and $\delta\tilde{\mathbf{U}}$ is an N dimensional vector.

If r is the rank of the response matrix $\mathbf{A}$ then the norm of the pseudoinverse, $\mathbf{A}^+$, is the inverse of singular value number r (of $\mathbf{A}$), i.e.,

$$\|\mathbf{A}^+\|_{l_2} = \frac{1}{\tau_r}, \tag{39}$$

where τ_r is the singular value number r, if the singular values are ordered in a decreasing sequence, i.e., singular-value number r is the smallest. The l_2-norm of $\mathbf{A}$ is the first-singular value of $\mathbf{A}$, i.e.,

$$\|\mathbf{A}\|_{l_2} = \tau_1, \tag{40}$$

Numerical values for $\|\mathbf{D}[\mathbf{W}(\mathbf{x})]\|_{l_2}$, $\|\mathbf{A}^+\|_{l_2}$ and ultimately equation (38) in one case are given in section 8.

8. EXPERIMENTAL TEST CASE

In this section the hybrid strain analysis (HSA) proposed in section 5 is validated experimentally on a test plate by comparison with independent strain measurements. The test plate consists of an aluminium plate glued to a Plexiglas, polymethyl methacrylate (PMMA), plate. The dimensions of the plate are $0{\cdot}630 \times 0{\cdot}300 \times 0{\cdot}0118$ m ($x \times y \times z$) with a rectangular cutout having dimensions $0{\cdot}330 \times 0{\cdot}100 \times 0{\cdot}0118$ m. The thicknesses of the two materials are 0·0076 and 0·0042 m for Plexiglas and aluminium respectively. The test plate in question is depicted in Figure 1, where the finite element mesh can also be seen. The finite element mesh consists of 4680 (solid) elements, with 20 nodes in each element. The total number of nodes is 24 430, with seven nodes through the thickness. In the Plexiglas two elements were used through the thickness, and for the aluminium only one was used.

The elastic eigenvalue problem was solved by means of ASKA Acoustics ([17]). A total number of 89 eigenvalues were solved using the Block Lanczos algorithm.

A very accurate measurement of weight and volume gave $\rho_{Al} = 2795\ \text{kg/m}^3$ and $\rho_{PMMA} = 1181\ \text{kg/m}^3$ for aluminium and Plexiglas respectively. For the aluminium plate the zero frequency Young's modulus and the Poisson ratio were estimated to $E_{Al} = 73{\cdot}0$ GPa and $\nu_{Al} = 0{\cdot}3260$, respectively, while for Plexiglas $E_{PMMA} = 3{\cdot}44$ GPa and $\nu_{PMMA} = 0{\cdot}3820$.

The measurements of the test plate were carried out using a laser Doppler vibrometer (LDV), in the frequency range 0·215–1024 Hz. Mobility frequency response functions in z direction (normal to the plate surface) for 75 different locations randomly distributed on the Plexiglas side, but such that they cover the plate with measurement intervals in x and y directions which are small enough for use of all modes up to mode number 60.

The plate was hanging in thin threads and excited with an electrodynamic shaker at a location near the centre of gravity. Strain measurements, for validation purpose, were made at two different locations on the aluminium side of the plate by means of strain gauges. TOYODA SEMICONDUCTORS type Sp-5-120B strain gauges are used. The shaker was mounted on the aluminium side, while mobility measurements using LDV were made normal to the Plexiglas side. One big advantage with measurements using laser Doppler vibrometer (LDV) instead of conventional gauges such as accelerometers and

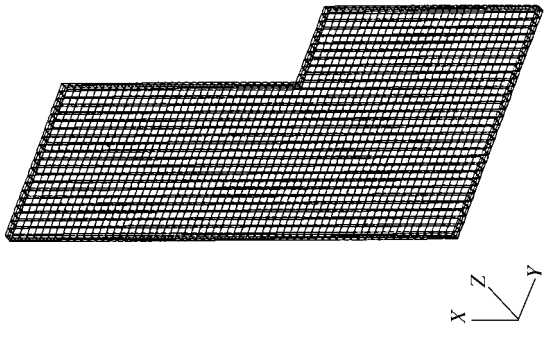

Figure 1. The test plate with finite element mesh. The Plexiglas in facing downwards, i.e., in the negative z direction.

TABLE 1

Co-ordinates of validation, estimation and excitation points

Point no.	FE node no.	x-co-ord. (m)	y-co-ord. (m)	z-co-ord. (m)	Comment
120	5731	0·1200	0·1800	0·0118	Strain gauge
195	13 985	0·3000	0·1400	0·0118	Excitation
196	14 721	0·3200	0·1400	0·0000	Validation
291	11 154	0·2400	0·0800	0·0118	Strain gauge
—	11 153	0·2400	0·0800	0·0076	Interface point
—	11 156	0·2400	0·0800	0·0000	Plexiglas side

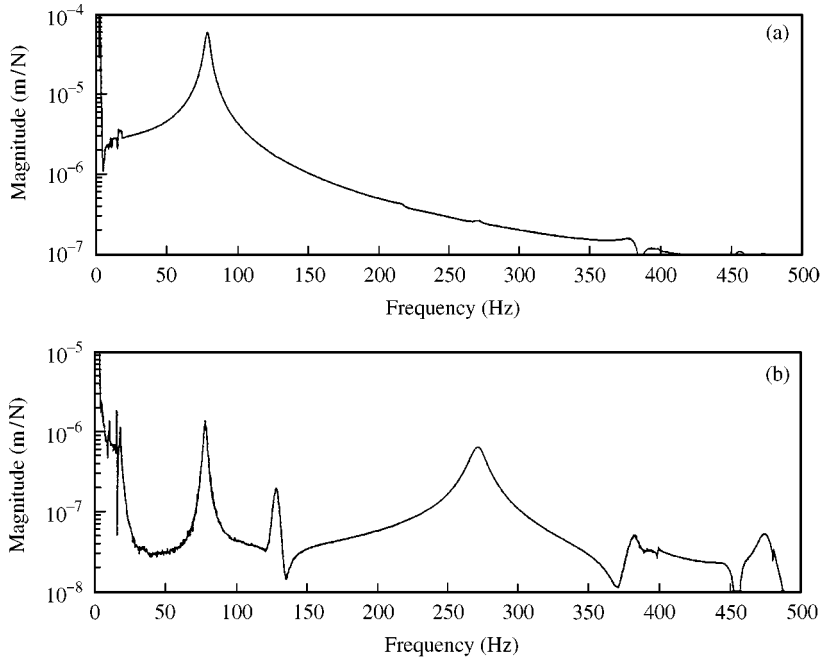

Figure 2. (a) Estimated Fourier coefficient spectrum for mode number 7, with elastic eigenfrequency $f_7 = 70$ Hz; (b) estimated Fourier coefficient spectrum for mode number 10, with elastic eigenfrequency $f_{10} = 238$ Hz.

strain gauges, is that a response can be obtained without interfering with the vibrations of the structure.

The locations of the shaker and strain gauges can be seen in Table 1.

The HSA was carried out on the data from LDV measurements, transformed to displacements, using ASKA-computed normal modes. Estimated Fourier coefficients for modes 7 and 10 are depicted in Figure 2. The mode coupling between modes 7 and 10 can be seen by the dominating peaks at 78 Hz for both spectra. The number of modes M, as in the modal expansion (6), was chosen to be 22. A comparison with the case of no residual in the displacement prediction is depicted in Figure 3. As can be seen the predicted result with residual give better agreement with the measurement, and hence the residual may be used in HSA.

The displacements to be used in the finite difference schemes were predicted. A total of five points, uniformly distributed around point 291, were used to calculate the strain ($\tilde{\varepsilon}_{22}$) at

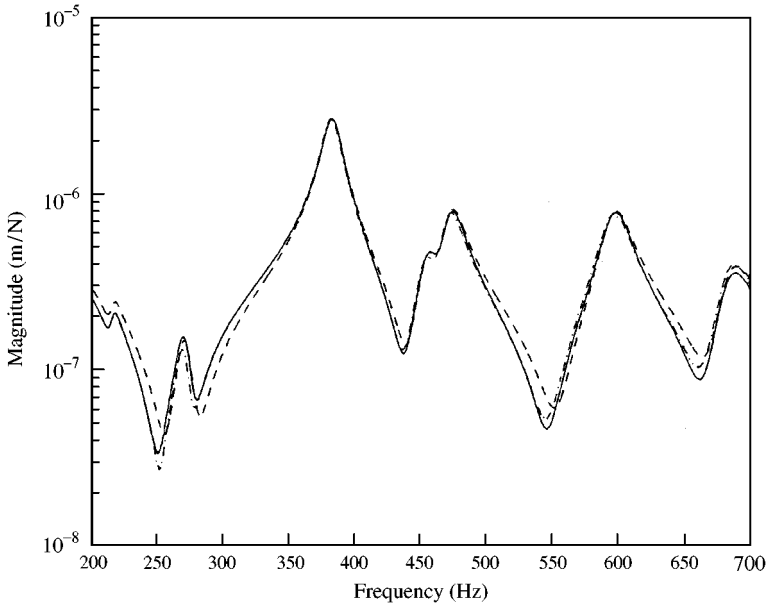

Figure 3. Predicted displacement at point 196 (on the Plexiglas side), not used in HMA, using residual and not: ——, predicted with 22 modes and residual; – – –, predicted with 22 modes and no residual; ·—·—, measured.

point 291. The result is depicted in Figure 4(a) with the measured strain response. The coherence for the measurement was good at almost every frequency, as can be seen in Figure 4(b), above 10 Hz and below 750 Hz.

Measurement error bounds for the calculated strain tensor at point 291 may be estimated using the theory in section 7. The rank of the response matrix $\mathbf{A}$ is 16, since 22 modes were used in HSA and six of them were rigid-body modes. The Fourier coefficients for the rigid-body modes were calculated using equation (22). According to equation (39) and with $\tau_{16} = 3{\cdot}6341$ $\|\mathbf{A}^+\|_{l_2} = 1/\tau_{16} = 0{\cdot}2752$. The l_2-norm of $\mathbf{D}[\mathbf{W}(\mathbf{x})]$ is, by use of equation (40), $\|\mathbf{D}[\mathbf{W}(\mathbf{x})]\|_{l_2} = 2{\cdot}0799$. Using equation (38) now gives $\|\delta\tilde{\boldsymbol{\varepsilon}}\|_{l_2} \leqslant 0{\cdot}5724 \cdot \|\delta\tilde{\mathbf{U}}\|_{l_2}$.

The predicted strain at point 291 corresponds well to the measured strain in almost every frequency interval except the first 30 Hz. As can be seen in Figure 4(a) the measured strain approaches 4×10^{-8}, while the predicted strain increases when the frequency approaches zero. When decreasing the number of modes, M, included in the Fourier coefficient estimation (making the HMA equation more overdetermined), the predicted strain spectrum converged to the measured strain spectrum. The conclusion is that the signal-to-noise ratio, in the LDV measurements used as input to the HMA, was too small for the strain predictions in the low-frequency region to be good.

For point 120 the strain was measured along a direction rotated 45° in the positive direction around the z-axis. The strain tensor was predicted using HSA and thereafter transformed so that the new y-axis was parallel to the measured direction. The co-ordinate transformation involves the use of $\tilde{\varepsilon}_{11}$, $\tilde{\varepsilon}_{22}$ and $\tilde{\varepsilon}_{12}$ which were predicted. As can be seen in Figure 5(a) the measured strain, $\varepsilon_{45°}$, corresponds well to the predicted; hence, in particular, the predicted $\tilde{\varepsilon}_{12}$ is correct. $\tilde{\varepsilon}_{12}$ is impossible to measure, and therefore co-ordinate transformation is the only way to verify the predicted $\tilde{\varepsilon}_{12}$. As for the measurement of point 291 the measurement at point 120 is acceptable, above 10 Hz and below 750 Hz, as can be seen in Figure 5(b).

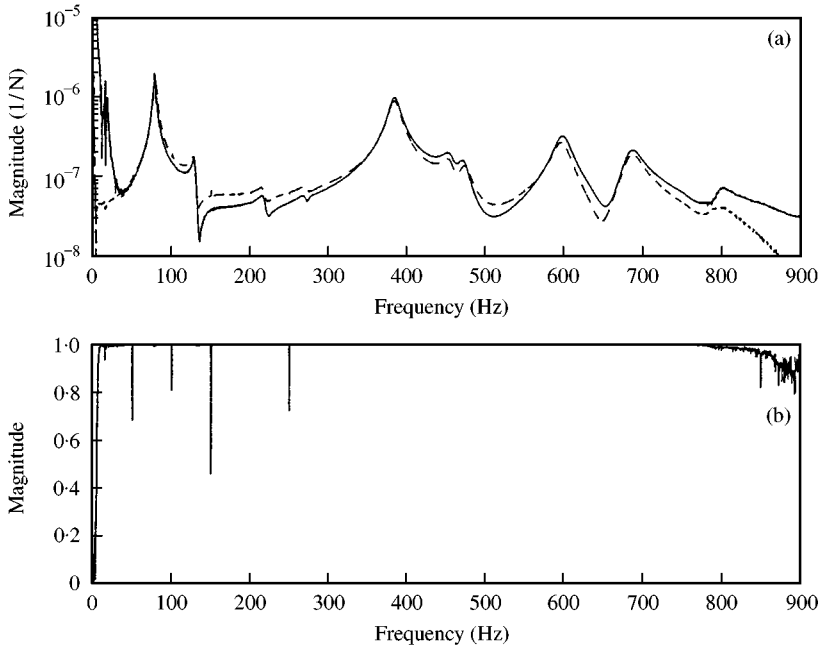

Figure 4. (a) Predicted and measured strain ($\tilde{\varepsilon}_{22}$) FRF at point 291 (at the aluminium side); (b) coherence for measured strain ($\tilde{\varepsilon}_{22}$) FRF at point 291: ——, predicted strain; – – –, measured strain.

Since strain measurements inside the structure cannot be performed, HSA predicted strain at node 11 153 (i.e., the node between the two materials) is compared with direct finite element computations. Displacement FRFs, only from the Plexiglas side, were used in the (five point) finite difference schemes for obtaining the strain tensor. The anelastic material properties for the Plexiglas used in the direct FE-computation were estimated with the method proposed by Dalenbring [2]. A total of 50 frequency responses, in the interval [10,500] Hz, were calculated. The predicted $\tilde{\varepsilon}_{11}$ is depicted in Figure 6, where it can be seen that the agreement between HSA predicted strain and direct FE-computation is very good. Here strain tensor assessment by direct FE-computation is interpreted as finite difference schemes, for obtaining the strain tensor, applied on direct FE-computed displacements. For $\tilde{\varepsilon}_{33}$ the agreement with direct FE-computation is not as good, as can be seen in Figure 7.

In all of the above examples the number of measurements was 75. As a comparison the number was reduced to 18, distributed so that only elastic modes up to mode number 22 could be resolved. The result when applying HSA is almost as good as before, as is depicted in Figure 8. However, it must be emphasized that the spatial distribution of measurements is on the limit for resolving elastic mode number 22.

The above examples demonstrate the HSA predicted strains agree well with measured ones. The analysis was based on known elastic (zero frequency) material properties for both materials. The question as to what happens if the elastic material properties of the plate is unknown, and furthermore, if not even the fact that the test plate is composed of two different kinds of materials, with different elastic (zero frequency) material properties, is posed. Assume that mean values for the true mass distribution, Young's modulus and the Poisson ratio of the two materials were to be used for the whole plate when calculating the normal modes. That is, the whole plate is assumed to have the following material properties: $\rho = 1988$ kg/m^3, $E = 38{\cdot}22$ GPa and $\nu = 0{\cdot}3540$. The HSA was carried out using 15 modes,

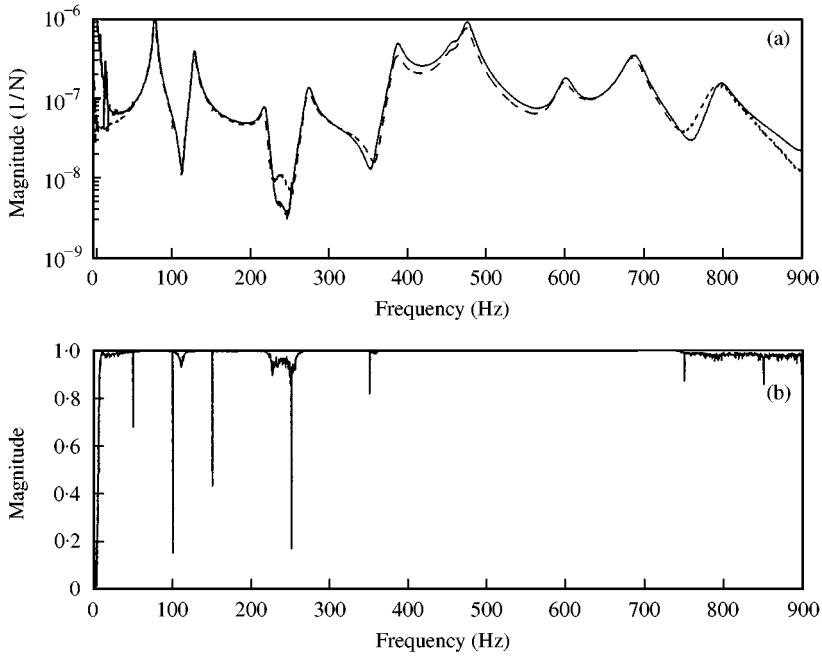

Figure 5. (a) Predicted and measured strain ($\tilde{\varepsilon}_{45^\circ}$) FRF at point 120 (on the aluminium side); (b) coherence for measured strain ($\tilde{\varepsilon}_{45^\circ}$) FRF at point 120: ——, predicted strain; – – –, measured strain.

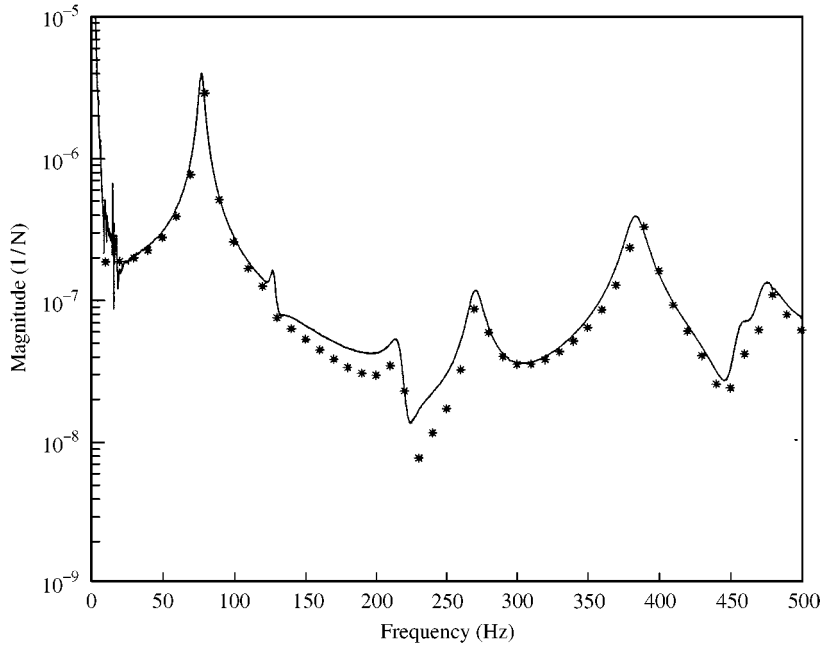

Figure 6. Predicted ($\tilde{\varepsilon}_{11}$) FRF at node 11 153, i.e., the node on the inferface between the two materials. Direct FE calculation uses estimated anelastic properties for the Plexiglas: ——, predicted using 22 modes; ∗, direct FE calculation.

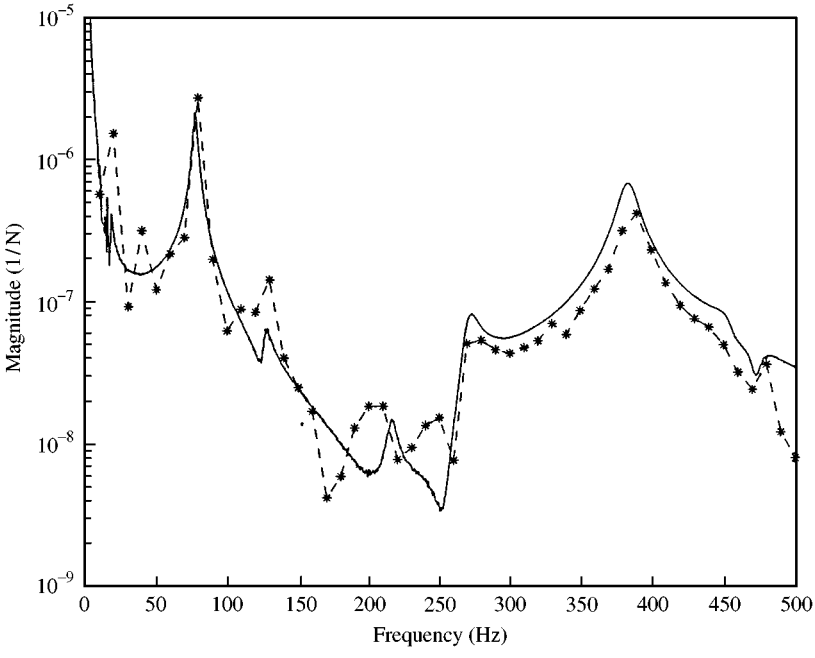

Figure 7. Predicted ($\tilde{\varepsilon}_{33}$) FRF at node 11 153, i.e., the node on the interface between the two materials. Direct FE calculation uses estimated anelastic properties for the Plexiglas: ——, predicted using 22 modes; ∗, direct FE calculation.

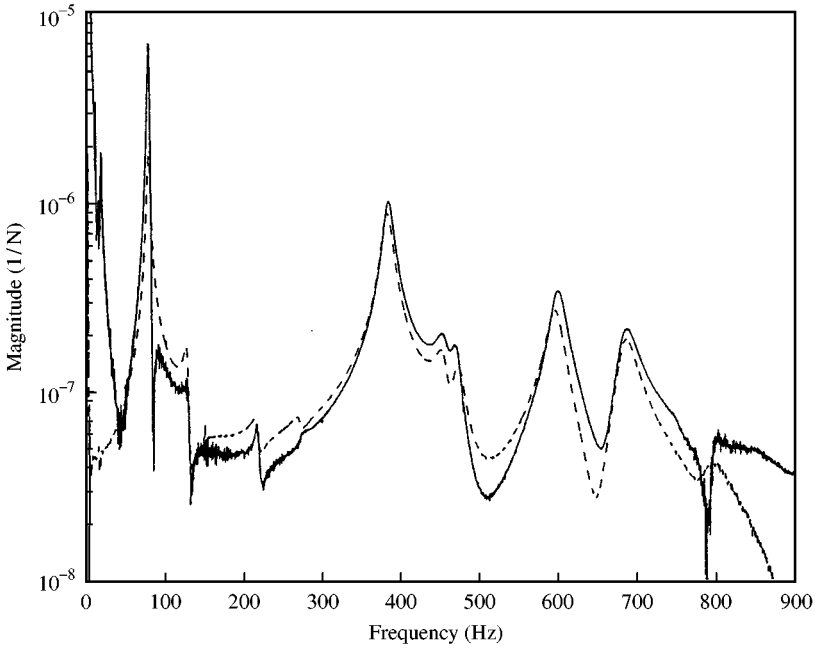

Figure 8. Predicted and measured strain ($\tilde{\varepsilon}_{22}$) FRF at point 291 (on the aluminium side). HSA is based on 18 measured FRF: ——, predicted strain using 18 measured FRF in HSA; – – –, measured strain.

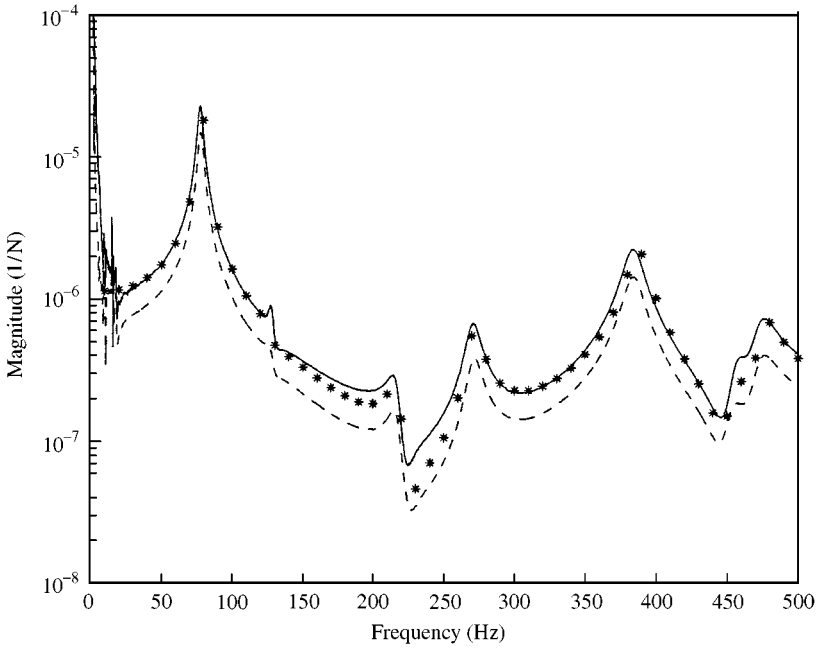

Figure 9. Predicted ($\tilde{\varepsilon}_{11}$) FRF at node 11 156, i.e., on the Plexiglas side. Strain predicted with correct material properties (——) is based on 22 modes; strain predicted with assumed material properties (– – –) is based on 15 modes. Direct FE calculation uses estimated anelastic properties for the Plexiglas: ——, predicted using correct (measured) material properties; – – –, predicted using assumed material properties; ∗, direct FE calculation.

i.e., $M = 15$. The result for strain predicted at point 291 on the Plexiglas side (i.e., node 11 156) can be seen in Figure 9, where it is compared with HSA predicted strain with correct (measured) material properties and direct FE computation. As before, the anelastic material properties for the Plexiglas used in direct FE computation were estimated using the method proposed by Dalenbring [2]. The predicted strain using arbitrary material properties agrees quite well. It must be kept in mind that in the z direction (i.e., through the thickness) measurement was only made at $z = 0$, hence it is hard to predict strain which depends on the variation through the thickness (i.e., $\tilde{\varepsilon}_{33}$, $\tilde{\varepsilon}_{23}$ and $\tilde{\varepsilon}_{31}$). Also the number of measurements, N, have not been increased, which it should in order to describe the discontinuity of the strain tensor.

9. SUMMARY

Based on vibration response measured at a limited number of points and numerical approximations to continuous Hilbert space basis functions combined with spatial differentiation, the strain tensor field, in the frequency domain, can be obtained by use of the method proposed in this paper. Essentially, results from HMA are transformed from the displacement space to the strain space by use of finite difference schemes.

The HMA technique provides a method of calculating the displacement vector, $\tilde{\mathbf{u}}$, at arbitrary points in the vibrating structure. This is obtained using a least-squares fit of the Fourier coefficients (or modal co-ordinates), $c_m(\tilde{\mathbf{u}})$, in the mode series expansion from a restricted set of measured vibration responses. Finite difference schemes enable

calculation of the strain tensor, from the displacement vector, at arbitrary points, to a desired accuracy.

The proposed method is applicable to a vibrating structure, regardless of the material properties of the body. Hence, any possible damping, e.g., material damping, damping in joints between structural parts, etc., need not be known *a priori*. Moreover, the zero frequency elastic properties and mass distribution of the structure need not be the true ones; any (meaningful) arbitrary values of the elastic properties and mass distribution can be assumed in order to obtain the Hilbert space basis functions, $\mathbf{w}^{(m)}$. Material inhomogeneities present (as for a piecewise continuous structure) may cause the method (when applied with unknown properties) to be inaccurate in the vicinity around the discontinuity. The model derived is valid for a specific excitation, not necessarily known.

The minimum number and distribution of measurement points is a matter of the shortest wavelength for the set of displacement modes, $\mathbf{w}^{(m)}$ $m \in [1, \ldots, M]$, to be used in the mode series expansion of the displacement field.

When applied to an experimental test case, the proposed method is in good agreement with both measured strain responses and strain responses obtained by direct FE calculation.

ACKNOWLEDGMENTS

This work was performed under contact from the Swedish Defence Material Administration (Contract no. 23250-93102-24-001). The funding provided is gratefully acknowledged.

The author would like to thank all staff at the Department of Structural Dynamics and Vibroacoustics at The Aeronautical Research Institute of Sweden (FFA) for encouragement and assistance. Especially, I am deeply in debt to Krister Dovstam (FFA) and Prof. Peter Göransson (Royal Institute of Technology and FFA) for all their advice and engaging and productive discussions.

REFERENCES

1. K. Dovstam 1998 *Computational Mechanics* **21**, 493–511. Real modes of vibration and hybrid modal analysis.
2. M. Dalenbring 1999 *Mechanical Systems and Signal Processing* **13**, 547–569. Damping function estimation based on measured vibration frequency responses and finite-element displacement modes.
3. K. Dovstam 1998 *Ph.D. Thesis, Royal Institute of Technology (KTH), Stockholm, Sweden*. On material damping modeling and modal analysis in structural dynamics.
4. O. Bernasconi and D. J. Ewins 1989 *Journal of Modal Analysis* **4**, 69–76. Modal strain/stress fields.
5. L. Koss and D. Karczub 1995 *Journal of Sound and Vibration* **184**, 229–244. Euler beam bending wave solution predictions of dynamic strain using frequency response functions.
6. M. Camden and L. Simmons 1998 *Proceedings of SPIE Conference on Laser Interferometry IX: Applications, San Diego, CA, July* 22–23, 311–318. Using a laser vibrometer for monitoring dynamic strain, modal analysis and calculating damping.
7. D. G. Karczub and M. P. Norton 1999 *Journal of Sound and Vibration* **226**, 675–700. Finite differencing methods for the measurement of dynamic bending strain.
8. J. M. Cuschieri 1991 *Noise Control Engineering Journal* **37**, 97–107. Experimental measurement of structural intensity on an aircraft fuselage.
9. B. C. Lee and K. J. Kim 1999 *Journal of Sound and Vibration* **228**, 845–856. Shear and normal strain effects of core layers in vibration of square sandwich plates under clamped boundary conditions.

10. K. DOVSTAM 1995 *International Journal of Solids and Structures* **32**, 2835–2852. Augmented Hooke's law in frequency domain. A three dimensional, material damping formulation.
11. D. J. EWINS 1986 *Modal Testing*: *Theory and Practice*. Letchworth: Research Studies Press Ltd.
12. K. DOVSTAM 1997 *International Journal of Solids Structures* **34**, 2733–2754. Receptance model based on isotropic damping functions and elastic displacement modes.
13. R. D. RICHTMYER 1978 *Principles of Advanced Mathematical Physics*, Vol. I, New York: Springer-Verlag.
14. G. MASE 1970 *Continuum Mechanics*. New York: McGraw-Hill.
15. N. SEHLSTEDT 1999 *M.Sc. Thesis*, *Chalmers University of Technology*, *Göteborg*, *Sweden*. Hybrid strain analysis based on numerical differentiation.
16. K. R. HOLLAND and F. J. FAHY 1997 *Noise Control Engineering Journal* **45**, 217–221. An investigation into spatial sampling criteria for use in vibroacoustic reciprocity.
17. P. GÖRANSSON 1988 *The Aeronautical Research Institute of Sweden FFA TN*, 1988-13. ASKA Acoustics. Theory and applications.
18. M. E. GURTIN 1972 in *Encyclopedia of Physics*, Vol. VIa/2, *Mechanics of Solids* II (S. Flügge and C. Trusdell, editors). Berlin: Springer-Verlag. The linear theory of elasticity.

APPENDIX A: DEFINITIONS

The displacement field, $\mathbf{u}$, the Voight-matrix representation of the symmetric stress tensor field, $\boldsymbol{\sigma}$, and strain tensor field, $\boldsymbol{\varepsilon}$, in Cartesian co-ordinates are defined as

$$\mathbf{u} = \mathbf{u}(\mathbf{x}, t) = [u_1\ u_2\ u_3]^{\mathrm{T}}, \tag{A.1}$$

$$\boldsymbol{\sigma} = \boldsymbol{\sigma}(\mathbf{x}, t) = [\sigma_{11}\ \sigma_{22}\ \sigma_{33}\ \sigma_{12}\ \sigma_{23}\ \sigma_{31}]^{\mathrm{T}}, \tag{A.2}$$

$$\boldsymbol{\varepsilon} = \boldsymbol{\varepsilon}(\mathbf{x}, t) = [\varepsilon_{11}\ \varepsilon_{22}\ \varepsilon_{33}\ 2\varepsilon_{12}\ 2\varepsilon_{23}\ 2\varepsilon_{31}]^{\mathrm{T}}, \tag{A.3}$$

where $\mathbf{x} = [x_1, x_2, x_3]^{\mathrm{T}}$ and t is the time variable.

The linear strain–displacement field relations are given as

$$\varepsilon_{ik} = \frac{1}{2}\left[\frac{\partial u_i}{\partial x_k} + \frac{\partial u_k}{\partial x_i}\right]. \tag{A.4}$$

Then the first order (strain), partial differential operator matrix can be defined as

$$\mathbf{D} = \begin{bmatrix} \dfrac{\partial}{\partial x_1} & 0 & 0 \\ 0 & \dfrac{\partial}{\partial x_2} & 0 \\ 0 & 0 & \dfrac{\partial}{\partial x_3} \\ \dfrac{\partial}{\partial x_2} & \dfrac{\partial}{\partial x_1} & 0 \\ 0 & \dfrac{\partial}{\partial x_3} & \dfrac{\partial}{\partial x_2} \\ \dfrac{\partial}{\partial x_3} & 0 & \dfrac{\partial}{\partial x_1} \end{bmatrix} \tag{A.5}$$

so that the strain field can be expressed as

$$\boldsymbol{\varepsilon} = \mathbf{D}[\mathbf{u}]. \tag{A.6}$$

The Cartesian matrix representation, $\mathbf{N} = \mathbf{N}(\mathbf{x})$, of the unit normal vector field, $\mathbf{n}(\mathbf{x}) = [n_1, n_2, n_3]^{\mathrm{T}}$, is defined as

$$\mathbf{N} = \begin{bmatrix} n_1 & 0 & 0 & n_2 & 0 & n_3 \\ 0 & n_2 & 0 & n_1 & n_3 & 0 \\ 0 & 0 & n_3 & 0 & n_2 & n_1 \end{bmatrix}. \tag{A.7}$$

The Cartesian traction vector is defined as

$$\mathbf{t}_n = \mathbf{N}\boldsymbol{\sigma}. \tag{A.8}$$

The $\mathbf{L}_2^3(\Omega) = L_2(\Omega) \times L_2(\Omega) \times L_2(\Omega)$ inner product $(\mathbf{u}, \mathbf{v})$ is defined as [13]

$$(\mathbf{u}, \mathbf{v}) = \int_\Omega \mathbf{u} \cdot \mathbf{v}^* \, \mathrm{d}\Omega = \int_\Omega (u_1 v_1^* + u_2 v_2^* + u_3 v_3^*) \, \mathrm{d}\Omega, \tag{A.9}$$

where $\mathbf{u}$ and $\mathbf{v}$ are some continuous functions, and $\mathbf{v}^*$ denotes the complex conjugate of the three-dimensional vector field $\mathbf{v}$. The inner product for vector fields on the boundary, $\partial\Omega$, is defined as

$$(\mathbf{u}, \mathbf{v})_\partial = \int_{\partial\Omega} \mathbf{u} \cdot \mathbf{v}^* \, \mathrm{d}\partial\Omega. \tag{A.10}$$

The natural norm in $\mathbf{L}_2^3(\Omega)$ is then defined as

$$\|\tilde{\mathbf{u}}\|_{\mathbf{L}_2^3(\Omega)} = \sqrt{(\tilde{\mathbf{u}}, \tilde{\mathbf{u}})} = \sqrt{\int_\Omega |\tilde{\mathbf{u}}|^2 \, \mathrm{d}\Omega}. \tag{A.11}$$

The mean value of the displacement, $\tilde{\mathbf{u}}_{mean}$, over an arbitrary, finite spatial volume, Ω_p, containing the point $\mathbf{p}$ is defined as

$$\tilde{\mathbf{u}}_{mean} = \frac{1}{\mathrm{Vol}(\Omega_p)} \int_{\Omega_p} \tilde{\mathbf{u}}(\mathbf{x}, s) \, \mathrm{d}\Omega, \tag{A.12}$$

where $\mathrm{Vol}(\Omega_p)$ is the scalar volume of the set Ω_p.

For two six-dimensional vector fields, $\mathbf{E}$ and $\mathbf{V}$, the $\mathbf{L}_2^6(\Omega)$ inner product is denoted as $\langle \mathbf{E}, \mathbf{V} \rangle$ and defined analogous to the above. The $\mathbf{L}_2^6(\Omega)$ norm is analogous to equation (A.11), i.e.,

$$\|\mathbf{E}\|_{\mathbf{L}_2^6(\Omega)} = \sqrt{\langle \mathbf{E}, \mathbf{E} \rangle}. \tag{A.13}$$

The mean value, $\mathbf{E}_{mean}$, of $\mathbf{E}$ is defined in analogy to equation (A.12).

The l_2-norm for an n-dimensional, real or complex, vector $\mathbf{y} = [y_1, y_2, \ldots, y_n]$ is defined as

$$\|\mathbf{y}\|_{l_2} = \sqrt{\sum_{i=1}^{n} |y_i|^2}. \tag{A.14}$$

When $\mathbf{y}$ is a real vector and the above norm is the well-known Euclidean norm. The corresponding l_2-matrix norm for a matrix $\mathbf{A}$, of order $n \times n$, is defined as

$$\|\mathbf{A}\|_{l_2} = \sup_{\mathbf{y} \neq \mathbf{0}} \frac{\|\mathbf{A}\mathbf{y}\|_{l_2}}{\|\mathbf{y}\|_{l_2}}. \tag{A.15}$$

The isotropic, elastic generalized Hooke's law relating the elastic stress vector with the strain vector can be expressed as

$$\mathbf{H} = \lambda \cdot \mathbf{H}_\lambda + G \cdot \mathbf{H}_G, \tag{A.16}$$

where $\lambda = 2\nu G/(1 - 2\nu)$, $G = E/(2(1 + \nu))$, $(\mathbf{H}_\lambda)_{ik} = 1$ for $i, k \leqslant 3$, and $(\mathbf{H}_G)_{ii} = 2$ for $i \leqslant 3$ and $(\mathbf{H}_G)_{ii} = 1$ for $4 \leqslant i \leqslant 6$.

The three-dimensional real-valued vector field $\mathbf{w}^{(m)} \in \mathbb{R}^3$ is the mode shape number m with corresponding circular eigenfrequency ω_m, i.e., $\mathbf{w}^{(m)}$ is assumed to be the solution to an elastic eigenvalue problem with equations of motion

$$-\mathbf{D}^{\mathrm{T}}\mathbf{H}\mathbf{D}[\mathbf{w}^{(m)}] = \omega_m^2 \rho \mathbf{w}^{(m)} \tag{A.17}$$

and homogeneous boundary conditions fulfilling

$$(\mathbf{N}\mathbf{H}\mathbf{D}[\mathbf{w}^{(m)}], \mathbf{w}^{(r)})_\partial = 0 \quad \forall m, r. \tag{A.18}$$

Due to these assumptions it is guaranteed that the continuous (real) modes of vibration constitute a set of complete basis functions in the Hilbert space $\mathbf{L}_2^3(\Omega)$ [18]. In addition to completeness, the modes are orthogonal

$$(\mathbf{w}^{(m)}, \rho \mathbf{w}^{(r)}) = a_m \delta_{mr}, \quad \forall m, r, \tag{A.19}$$

where δ_{mr} is the Kronecker delta.

APPENDIX B: PROPERTIES OF THE STRAIN OPERATOR D

The operator, $\mathbf{D}$, as defined in Appendix A, is a map from the three-dimensional displacement space to a subspace of the six-dimensional strain space. The linearity of $\mathbf{D}$ follows directly from the definition.

Let $\mathscr{A}$ be a set of functions, $u_i(\mathbf{x}, s)$, such that the partial derivatives exist and are continuous in Ω, except on a finite number of interfaces where material discontinuities are present. Then the domain of definition for $\mathbf{D}$ is

$$\mathscr{D}(\mathbf{D}) = \{\mathbf{u}(\mathbf{x}, s) \in \Omega \,|\, u_i(\mathbf{x}, s) \in \mathscr{A},\ i = 1, 2, 3\}, \tag{B.1}$$

where $\mathbf{u}(\mathbf{x}, s)$ is the three-dimensional displacement field defined in Appendix A, and $\Omega \subset \mathbb{R}^3$ is a compact, i.e., closed and bounded, set describing the three-dimensional solid under study. The situation with a solid structure implies a continuous displacement field. The continuity of the displacement field, in turn, implies bounded spatial derivatives.

The operator, $\mathbf{D}$, can be decomposed into three linear mappings, $\mathbf{M}_i$ $i = 1, 2, 3$, and three partial differential operators defined as

$$D_i[\mathbf{u}] = \left[\frac{\partial u_1}{\partial x_i}, \frac{\partial u_2}{\partial x_i}, \frac{\partial u_3}{\partial x_i}\right]^{\mathrm{T}}. \tag{B.2}$$

Every $\mathbf{M}_i$ is a 6×3 matrix with ones at positions corresponding to differentiation with respect to x_i in the operator $\mathbf{D}$, and zeros elsewhere.

Then $\mathbf{D}$ is explicitly as

$$\mathbf{D}[\mathbf{u}] = (\mathbf{M}_1 D_1 + \mathbf{M}_2 D_2 + \mathbf{M}_3 D_3)[\mathbf{u}]. \tag{B.3}$$

Taking the l_2-norm (see Appendix A) of the above equation, and using Cauchy–Schwarz' inequality, the triangle inequality and the fact that $\|\mathbf{M}_i\|_{l_2} = 1$ yields

$$\begin{aligned} \|\mathbf{D}[\mathbf{u}]\|_{l_2} &\leqslant \|D_1[\mathbf{u}]\|_{l_2} + \|D_2[\mathbf{u}]\|_{l_2} + \|D_3[\mathbf{u}]\|_{l_2} \\ &\leqslant K_1 \|\mathbf{u}\|_{l_2} + K_2 \|\mathbf{u}\|_{l_2} + K_3 \|\mathbf{u}\|_{l_2} \\ &= K \|\mathbf{u}\|_{l_2}, \end{aligned}$$

where the boundedness of each differential operator D_i was used, and each K_i and K are finite positive real numbers. Hence, with the domain of definition (B.1) the strain operator $\mathbf{D}$ is bounded at all points apart from a finite number of discontinuity surfaces, where material discontinuities are present.